A Single-Switch Quadratic Buck–Boost Converter With Continuous Input Port Current and Continuous Output Port Current

Neng Zhang, Guidong Zhang, *Member, IEEE*, Khay Wai See, and Bo Zhang, *Senior Member, IEEE*

***Abstract*—A single-switch quadratic buck–boost converter with continuous input port current and continuous output port current is proposed in this paper. Compared with the traditional buck-boost converter, the proposed converter can obtain a wider range of the voltage conversion ratio with the same duty cycle. Moreover, the proposed converter can operate with continuous input port current and continuous output port current compared to the existing counterparts with inherently discontinuous input port current and discontinuous output port current. The operating principle and steady-state performance of the proposed converter under continuous inductor current mode is analyzed in detail. Then, the comparison between the proposed converter and the existing quadratic buck–boost converters has been conducted to demonstrate the unique features of the proposed one. Finally, experimental results from a prototype built in the lab are recorded to verify the effectiveness and validity of the proposed quadratic buck–boost converter.**

***Index Terms*—Continuous input port current, continuous output port current, quadratic buck–boost converter, single-switch.**

I. Introduction

RENEWABLE energy such as photovoltaic (PV) panels and wind turbines are increasingly being used because of the environmental awareness and advances in technology with the decreasing manufacturing cost. Power electronics circuits are usually required to convert their output power to match the load demand. In some industrial applications, such as PV-supplied LED street lighting, the input voltage can vary significantly, while the output needs to be maintained constant. The variation in the input voltage can be much larger than the output. Also, some multifunctional power supplies need a wide range of output voltages while supplied by a constant input source. In these cases, a buck–boost DC/DC converter with wide gain is required. It is well known that the voltage conversion ratio M ($M = V_{\text{out}}/V_{\text{in}}$, where V_{out} is the output voltage and V_{in} is the input voltage) of the pulse width modulation DC–DC converters is a function of the duty cycle of the switch. The quadratic converter, whose voltage conversion ratio has a quadratic relationship in terms of the duty cycle, has the potential for the applications that require a wide input–output voltage conversion [1]–[3].

A lot of studies about quadratic buck converters [4]–[11] and quadratic boost converters [12]–[18] have been developed and reported. Therein, some researchers have studied the mathematical model and control methods for the quadratic buck converters [4]–[8], while others focused on the soft-switching techniques [9], [10]. Also, the reduction of redundant power processing approach was used to develop new quadratic buck converters [11]. Some novel quadratic boost converter topologies were also proposed and analyzed [13]–[18]. However, very few research works have been carried out on the topology of the quadratic buck–boost converter.

A cascaded quadratic buck–boost converter, which is shown in Fig. 1(a) and named the traditional quadratic buck–boost converter, has been proposed in [1] and [2]. This converter is formed by cascading two traditional buck–boost converters. It is obvious that the input port current of this converter i_{in} is equal

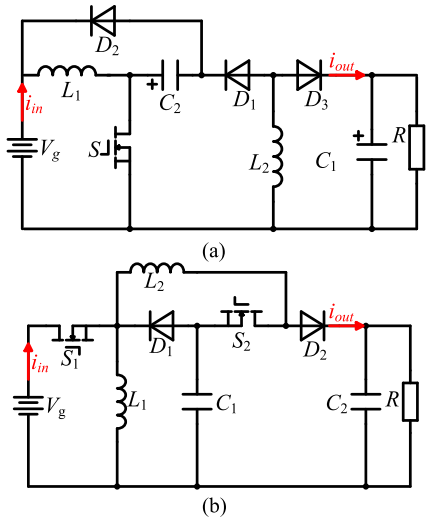

Fig. 1. Quadratic buck–boost converter proposed in (a) [1] and [2], (b) [19].

Manuscript received March 20, 2017; revised June 1, 2017; accepted June 13, 2017. Date of publication June 20, 2017; date of current version February 1, 2018. N. Zhang Ph.D. scholarship was supported by the China Scholarship Council and the University of Wollongong. Recommended for publication by Associate Editor G. Moschopoulos. *(Corresponding Author: Bo Zhang.)*

N. Zhang and K. W. See are with the Institute for Superconducting & Electronic Materials, University of Wollongong, Wollongong, N.S.W. 2522, Australia (e-mail: nz970@uowmail.edu.au; kwsee@uow.edu.au).

G. Zhang is with the School of Automation, Guangdong University of Technology, Guangzhou 510006, China (e-mail: zgdscut@gmail.com).

B. Zhang is with the School of Electric Power, South China University of Technology, Guangzhou 510641, China (e-mail: epbzhang@scut.edu.cn).

Color versions of one or more of the figures in this paper are available online at http://ieeexplore.ieee.org.

Digital Object Identifier 10.1109/TPEL.2017.2717462

See http://www.ieee.org/publications_standards/publications/rights/index.html for more information.

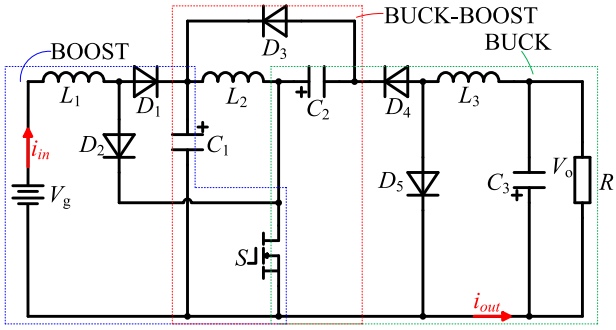

Fig. 2. Configuration of the proposed converter.

to the current of the inductor L_1 while the output port current i_{out} is zero when the switch is turned ON, the input port current is zero while the output port current is equal to the current of the inductor L_2 when the switch is turned OFF. Therefore, the input port current and the output port current of the traditional quadratic buck–boost converter are inherently discontinuous, which is possible to result in increased input and output current ripples and complicate the design of the input and output filters. Another transformer-less quadratic buck–boost converter has recently been proposed in [19] as shown in Fig. 1(b), in which two synchronously operating and floating connected switches are required. Meanwhile, similar as the traditional quadratic buck–boost converter, the input port current and the output port current of this converter are naturally discontinuous. Hence, it is of interest to develop novel quadratic buck–boost converters with single switch and continuous input port current and continuous output port current.

This paper is to propose a novel quadratic buck–boost converter, which combines one traditional boost converter, one traditional buck converter, and one traditional buck–boost converter using only one power switch. The proposed converter has a wider voltage conversion ratio than that of the traditional buck–boost converter. Compared with the quadratic buck–boost converters shown in Fig. 1, the proposed converter can operate with continuous input port current and continuous output port current, which can contribute to the simplification of the design of input and output filters.

The remainder of this paper is structured as follows. In Section II, the structure and operating principle of the proposed converter in continuous inductor current mode are presented. The steady-state performance of the converter is analyzed in Section III, which is followed by the comparisons between the proposed converter and the existing quadratic buck–boost converters given in Section IV. The design of key parameters of the components is derived briefly in Section V. Experimental results from a prototype built in the lab are given in Section VI to confirm the theoretical analysis and demonstrate the features of the proposed converter. Section VII concludes the paper.

II. Structure and Operation Principle of the Proposed Converter

The configuration of the proposed converter is shown in Fig. 2, in which a boost converter, a buck–boost converter, and

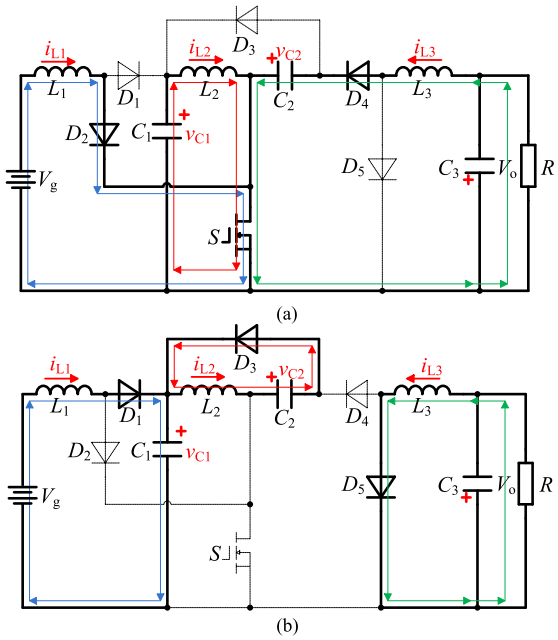

Fig. 3. Equivalent circuits of the proposed converter: (a) Mode1, (b) Mode2.

a buck converter are combined using only one switch, which contributes to a relative simple structure. The boost converter consists of input source V_{g}, diodes D_1 and D_2, inductor L_1, capacitor C_1, and switch S. The buck–boost converter consists of capacitors C_1 and C_2, inductor L_2, diode D_3, and switch S. The buck converter consists of capacitors C_2 and C_3, diodes D_4 and D_5, inductor L_3, switch S, and load R. It can be seen that the output capacitor of the boost converter is the input source of the buck–boost converter while the output of the buck–boost converter is the input source of the buck converter. It is of interest to note that there is an inductor connected in the input port and an inductor connected in the output port of the converter, which can contribute to the unique feature of drawing continuous input port current and continuous output port current.

To simplify the analysis of the operating principle of the proposed converter, some assumptions are made as follows:

1) all components are assumed to be ideal; and
2) all capacitors are large enough that the voltage across each capacitor is considered to be nearly constant during one switching period.

Similar to other buck–boost converters, the proposed converter can theoretically operate in both continuous inductor current mode and discontinuous inductor current mode. However, since the continuous inductor current mode is normally preferred in many industrial applications to reduce the current ripple and operating with continuous input, and output current is a main benefit of the proposed converter, it will be analyzed in continuous inductor current mode in this paper.

Based on the aforesaid assumptions, the converter will have two operating modes, i.e., mode 1 (S is turned ON) and mode 2 (S is turned OFF), in a single switching period. The equivalent circuits in the two operating modes are shown in Fig. 3(a) and (b). Some key waveforms of the proposed converter in a

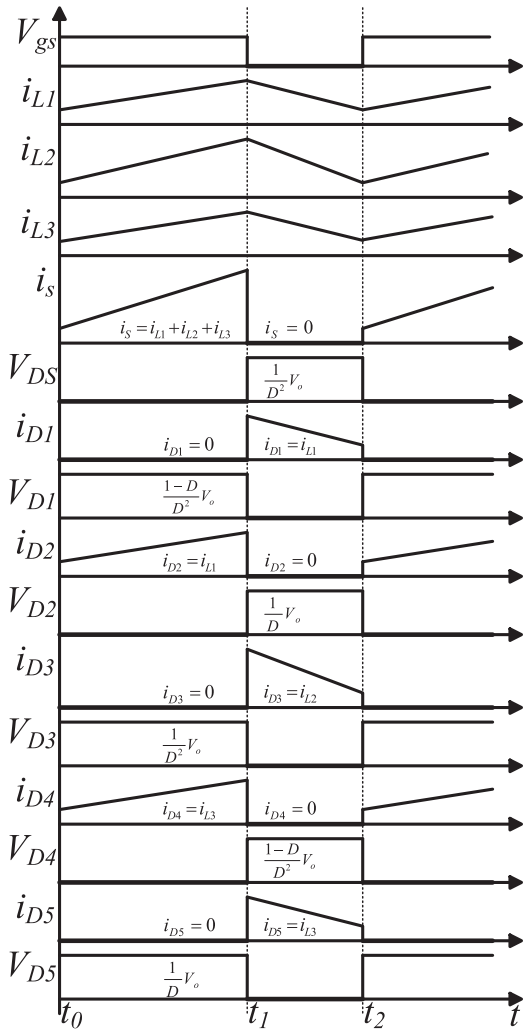

Fig. 4. Key waveforms of the proposed converter.

switching period are illustrated in Fig. 4 to show the operating processes. The two operating modes are described as follows:

Mode 1 [t_0-t_1]: As shown in Figs. 3(a) and 4, the switch *S* is conducting, diodes D_2 and D_4 are in ON state, and diodes D_1, D_3, and D_5 are reverse-biased by v_{C1}, $v_{C1} + v_{C2}$, and v_{C2}, respectively. The input source V_g delivers power to the inductor L_1 through the diode D_1 and the switch *S*, meantime, the energy stored in capacitors C_1 and C_2 is being released to inductors L_2 and L_3, respectively. Therefore, the currents flow through inductors L_1, L_2, and L_3, i.e., i_{L1}, i_{L2}, and i_{L3} are increasing. Some of the main equations among the components in this mode are as follows:

$$\begin{cases} L_1 \frac{di_{L1}}{dt} = v_g, \quad L_2 \frac{di_{L2}}{dt} = v_{C1}, \quad L_3 \frac{di_{L3}}{dt} = v_{C2} - v_o \\ C_1 \frac{dv_{c1}}{dt} = i_{L2}, \quad C_2 \frac{dv_{c2}}{dt} = i_{L3}, \quad C_3 \frac{dv_0}{dt} = i_{L3} - \frac{v_0}{R} \end{cases} \tag{1}$$

where v_{C1} represents the voltage of the capacitor C_1, v_{C2} is the voltage of the capacitor C_2, while v_o is the output voltage.

Mode 2 [t_1-t_2]: At t_1, the operating mode of the proposed converter changes to Mode 2 from Mode 1. As shown in Fig. 3(b), the switch *S* is turned OFF, diodes D_1, D_3, and D_5 are in ON state, and diodes D_2 and D_4 are reverse-biased by v_{C2} and v_{C1}, respectively, in this operating mode. The energy stored in the inductor L_1 as well as the input source is delivered to the capacitor C_1, and the capacitor C_1 starts to store energy. The inductor L_2 discharges energy to the capacitor C_2 through the diode D_3. At the same time, the inductor L_3 discharges energy to the capacitor C_3 and load *R*. Therefore, i_{L1}, i_{L2}, and i_{L3} are decreasing as shown in Fig. 4. Some of the main equations among the components in this mode are as follows:

$$\begin{cases} L_1 \frac{di_{L1}}{dt} = v_g - v_{C1}, L_2 \frac{di_{L2}}{dt} = -v_{C2}, L_3 \frac{di_{L3}}{dt} = -v_o \\ C_1 \frac{dv_{c1}}{dt} = -i_{L1}, C_2 \frac{dv_{c2}}{dt} = -i_{L2}, C_3 \frac{dv_0}{dt} = i_{L3} - \frac{v_0}{R} \end{cases}. \tag{2}$$

III. Steady-State Performance Analysis of the Proposed Converter

A. Ideal Voltage Conversion Ratio

To simplify the analysis, the converter is assumed to be a lossless system and the relationship of $V_g I_{in} = V_o I_o$ is held, where I_{in} and I_o are the input current and the output current, respectively. It is also assumed that the voltage ripples on all capacitors are zero. Moreover, the losses of the power devices such as the switch and the diodes are not considered.

Using the volt–second balance principle on the inductors and the ampere–second balance principle on the capacitors, the following equations can be obtained:

$$\begin{cases} V_g - V_{C1}(1-D) = 0 \\ V_{C1} D - V_{C2}(1-D) = 0 \\ V_{C2} D - V_o = 0 \\ I_{L2} D - I_{L1}(1-D) = 0 \\ I_{L3} D - I_{L2}(1-D) = 0 \\ I_{L3} - \frac{V_o}{R} = 0 \end{cases}. \tag{3}$$

From (3), the ideal output voltage and the voltages of the capacitors can be derived in terms of the input voltage V_g and the duty cycle *D* of the switch as

$$\begin{cases} V_{C1} = \frac{1}{1-D} V_g \\ V_{C2} = \frac{D}{(1-D)^2} V_g \\ V_o = \left(\frac{D}{1-D}\right)^2 V_g \end{cases}. \tag{4}$$

According to (4), the ideal voltage conversion ratio *M* of the proposed converter can be obtained as

$$M = \frac{V_o}{V_g} = \left(\frac{D}{1-D}\right)^2. \tag{5}$$

According to (5) and the expression of the ideal voltage conversion ratio of the traditional buck–boost converter, the relationship between the ideal voltage conversion ratio and the

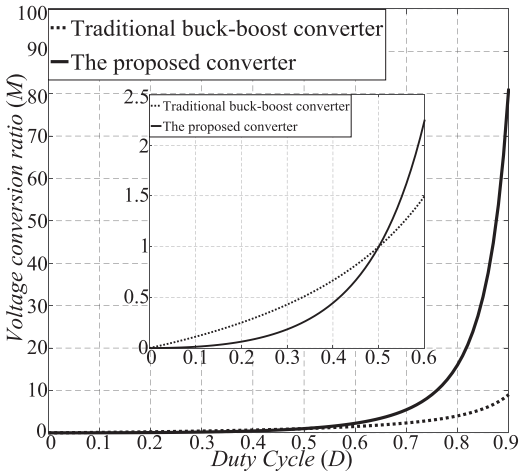

Fig. 5. Comparison of the ideal voltage conversion ratio between the proposed converter and the traditional buck–boost converter.

duty cycle of the proposed converter as well as the traditional buck-boost converter are plotted in Fig. 5. Fig. 5 shows that the proposed converter can obtain a wider voltage conversion ratio range than the traditional buck–boost converter.

B. Currents of the Inductors

The current ripples of the inductors, namely, Δi_{L1}, Δi_{L2}, and Δi_{L3} can be deduced as

$$\begin{cases} \Delta i_{L1} = \dfrac{V_g D}{L_1 f_s} = \dfrac{(1-D)^2 V_o}{D L_1 f_s} \\ \Delta i_{L2} = \dfrac{V_{C1} D}{L_2 f_s} = \dfrac{(1-D) V_o}{D L_2 f_s} \\ \Delta i_{L3} = \dfrac{(V_{C2} - V_o) D}{L_3 f_s} = \dfrac{(1-D) V_o}{L_3 f_s} \end{cases}. \tag{6}$$

From (3), the average currents of the inductors L_1, L_2, and L_3, namely, $I_{\mathrm{L1_{avg}}}$, $I_{\mathrm{L2_{avg}}}$, and $I_{\mathrm{L3_{avg}}}$, can be calculated as follows:

$$\begin{cases} I_{L1\_\mathrm{avg}} = (\frac{D}{1-D})^2 I_o \\ I_{L2\_\mathrm{avg}} = \dfrac{D}{1-D} I_o \\ I_{L3\_\mathrm{avg}} = I_o \end{cases}. \tag{7}$$

By manipulating (6) and (7), it can be derived that the inductances of the inductors must satisfy the following conditions to ensure that all the inductors operate in continuous current mode:

$$\begin{cases} L_1 > \dfrac{(1-D)^4 R}{2D^3 f_s} \\ L_2 > \dfrac{(1-D)^2 R}{2D^2 f_s} \\ L_3 > \dfrac{(1-D) R}{2 f_s} \end{cases} \tag{8}$$

where *R* is the load.

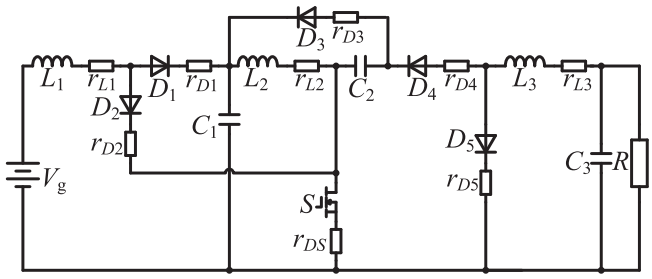

Fig. 6. Equivalent circuit of the converter considering parasitic parameters.

C. Analysis of Voltage and Current Stresses of Power Devices

According to the aforementioned analysis, the voltage stresses, average current of the switch *S*, and all diodes can be derived as follows.

The voltage stresses of diodes D_1 and D_4, namely, V_{D1} and V_{D4}, are equal to the voltage of the capacitor C_1, which can be expressed as

$$V_{D1} = V_{D4} = V_{C1} = \frac{1-D}{D^2} V_o. \tag{9}$$

Similarly, the voltage stresses of diodes D_2, D_3, D_5, and the switch *S*, namely, V_{D2}, V_{D3}, V_{D5}, and V_{DS}, can be expressed as

$$\begin{cases} V_{D2} = V_{D5} = V_{C2} = \dfrac{1}{D} V_o \\ V_{D3} = V_{\mathrm{DS}} = V_{C1} + V_{C2} = \dfrac{1}{D^2} V_o \end{cases}. \tag{10}$$

The average currents of the switch and diodes can be derived as follows:

$$\begin{cases} I_{S\_\mathrm{avg}} = \dfrac{D^3 - D^2 + D}{(1-D)^2} I_o, & I_{D3\_\mathrm{avg}} = D I_o \\ I_{D1\_\mathrm{avg}} = \dfrac{D^2}{1-D} I_o, & I_{D4\_\mathrm{avg}} = D I_o \\ I_{D2\_\mathrm{avg}} = \dfrac{D^3}{(1-D)^2} I_o, & I_{D5\_\mathrm{avg}} = (1-D) I_o \end{cases}. \tag{11}$$

D. Analysis of the Parasitic Parameters' Impacts

Considering the parasitic resistors of the inductors and power devices and the voltage drops of the power devices, the equivalent circuit of the converter can be drawn as shown in Fig. 6. In this figure, r_{L1}, r_{L2} and r_{L3} are parasitic resistances of inductors L_1, L_2 and L_3, respectively. r_{D1}– r_{D5} stand for the parasitic resistors of the diodes, and r_{DS} is the parasitic resistor of the switch. The voltage drops of the diodes and switch are represented by $V_{\mathrm{dr1}} - V_{\mathrm{dr5}}$, and V_{drS}, respectively.

According to the operating principle of the converter and applying volt–second balance principle on the inductors, the voltage relationships of V_{C1}, V_{C2}, V_{o} in terms of V_{g} and the

parasitic parameters can be derived as

$$V_{C1} = \frac{V_g - \frac{D^2}{(1-D)^2}\frac{V_o}{R}r_{L1} - \frac{D^2}{1-D}\frac{V_o}{R}r_{D1} - \frac{D^3}{(1-D)^2}\frac{V_o}{R}r_{D2} - \frac{(D^3-D^2+D)}{(1-D)^2}\frac{V_o}{R}r_{\mathrm{DS}} - V_{\mathrm{drS}}D - V_{\mathrm{dr2}}D - V_{\mathrm{dr1}}(1-D)}{(1-D)} \tag{12}$$

$$V_{C2} = \frac{V_{C1}D(1-D)^2 - D(1-D)\frac{V_o}{R}r_{L2} - D(1-D)^2\frac{V_o}{R}r_{D3} - (D^3-D^2+D)\frac{V_o}{R}r_{\mathrm{DS}} - V_{\mathrm{drS}}D(1-D)^2 - V_{\mathrm{dr3}}(1-D)^3}{(1-D)^3} \tag{13}$$

$$V_o = V_{C2}D - \frac{V_o}{R}r_{L3} - D\frac{V_o}{R}r_{D4} - (1-D)\frac{V_o}{R}r_{D5} - \frac{D^3-D^2+D}{(1-D)^2}\frac{V_o}{R}r_{\mathrm{DS}} - V_{\mathrm{drS}}D - V_{\mathrm{dr4}}D - V_{\mathrm{dr5}}(1-D). \tag{14}$$

Based on (12)–(14), the expression of the output voltage considering parasitic parameters can be obtained as

$$V_o = \frac{D^2(1-D)^2V_g - V_{\mathrm{drop}}}{M_3} \tag{15}$$

where

$$\begin{aligned} V_{\mathrm{drop}} &= V_{\mathrm{dr1}}D^2(1-D)^3 - V_{\mathrm{dr2}}D^3(1-D)^2 - V_{\mathrm{dr3}}D(1-D) \\ &\quad - V_{\mathrm{dr4}}D(1-D)^4 - V_{\mathrm{dr5}}(1-D)^5 \\ &\quad - V_{\mathrm{drS}}D(1-D)^2(D^2-D+1) \\ M_3 &= M_2(1-D) + D^4\frac{r_{L1}}{R} + D^4(1-D)\frac{r_{D1}}{R} \\ &\quad + D^5\frac{r_{D2}}{R} + (D^5-D^4+D^3)\frac{r_{\mathrm{DS}}}{R} \\ M_2 &= M_1(1-D) + D^2(1-D)\frac{r_{L2}}{R} + D^2(1-D)^2\frac{r_{D3}}{R} \\ &\quad + (D^4-D^3+D^2)\frac{r_{\mathrm{DS}}}{R} \\ M_1 &= (1-D)^2 + \frac{r_{L3}}{R}(1-D)^2 + D(1-D)^2\frac{r_{D4}}{R} \\ &\quad + (1-D)^3\frac{r_{D5}}{R} + (D^3-D^2+D)\frac{r_{\mathrm{DS}}}{R}. \end{aligned}$$

Comparing (4) and (15), the output voltage deviation ratio, which is the percentage of the difference between the ideal output voltage and the output voltage considering parasitic parameters to the ideal output voltage, can be obtained as

$$\sigma = \frac{M_3D^2V_g - D^2(1-D)^4V_g + (1-D)^2V_{\mathrm{drop}}}{M_3D^2V_g}. \tag{16}$$

If the load R is large enough comparing to the parasitic resistors of the components, the terms including r_{Lx}/R ($x = 1, 2, 3$), r_{Ly}/R ($y = 1, 2, 3, 4, 5, \mathrm{S}$) in M_1, M_2, and M_3 will be approaching zero. In this case, M_3 can be simplified as

$$M_3 = (1-D)^4. \tag{17}$$

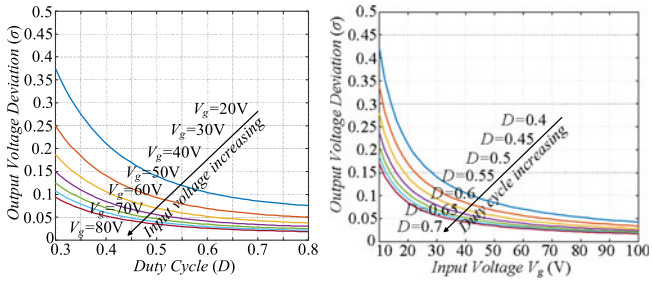

Fig. 7. Relationships between the output voltage deviation ratio and (a) duty cycle at different input voltages, (b) input voltage under different duty cycle conditions.

Substituting (17) into (15) and (16) and assuming the voltage drops of the diodes and the switch are equal to V_{drop} for simplification, the expression of the output voltage and the deviation ratio can be obtained as

$$V_o = \frac{D^2}{(1-D)^2}V_g - \frac{1+2D^3-D^2}{(1-D)^2}V_{\mathrm{drop}} \tag{18}$$

$$\sigma = \frac{1+2D^3-D^2}{D^2V_g}V_{\mathrm{drop}}. \tag{19}$$

It can be found from (19) that the output voltage deviation ratio is directly related to the input voltage and the duty cycle. Through doing partial derivative calculation of σ with respect to the duty cycle D and the input voltage V_{g}, respectively, the relationships shown in (20) can be obtained

$$\begin{cases} \dfrac{\partial\sigma}{\partial V_g} < 0 \\ \dfrac{\partial\sigma}{\partial D} < 0 \end{cases}. \tag{20}$$

The relationship among the output voltage deviation ratio, the duty cycle, and the input voltage can be further depicted in Fig. 7 by assuming that the parasitic parameters are constant during the operating process as $V_{\mathrm{drop}} = 0.7$ V. From (19), (20) and Fig. 7, it is found that the deviation ratio of the output voltage decreases significantly with the increase of the input voltage and the duty cycle. It should be claimed that the deviation ratio will become even smaller with the application of high-performance devices with better parasitic parameters.

The joule effect losses of the inductors, namely, P_L, can be approximately calculated as

$$P_{L\_\mathrm{con}} \approx \frac{r_{L1}D^4P_o}{(1-D)^4R} + \frac{r_{L2}D^2P_o}{(1-D)^2R} + \frac{r_{L3}P_o}{R} \tag{21}$$

where D is the duty cycle and P_{o} is the output power.

The conduction losses of the diodes and the switch, namely, $P_{\mathrm{DS\_}C}$, can be approximately calculated as

$$P_{\mathrm{DS\_}C} \approx \frac{r_{D1}D^5P_o}{(1-D)^4R} + \frac{r_{D2}D^4P_o}{(1-D)^3R} + \frac{r_{D3}D^2P_o}{(1-D)R}$$

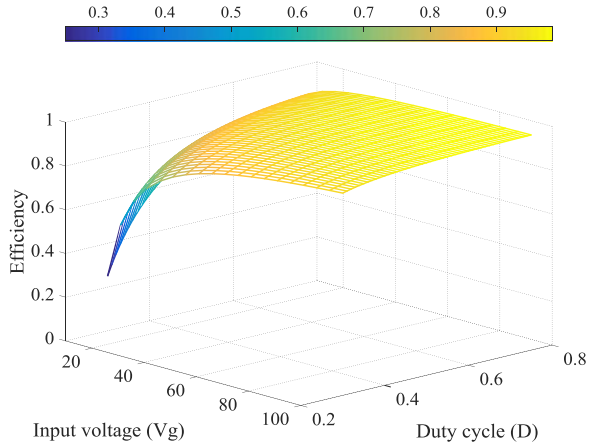

Fig. 8. Efficiency versus input voltage and duty cycle.

$$+\frac{r_{D4}D^3P_o}{R}$$
$$+\frac{r_{\mathrm{DS}5}(1-D)^3P_o}{R}+\frac{r_{\mathrm{DS}}(D^4-D^3+D^2)P_o}{(1-D)^2R}. \quad (22)$$

The losses of the diodes and the switch caused by the forward voltage drops, namely, $P_{\mathrm{DS\_dr}}$, can be approximately calculated as

$$P_{\mathrm{DS}\_dr}\approx\frac{V_{\mathrm{dr}1}D^2P_o}{(1-D)V_o}+\frac{V_{\mathrm{dr}2}D^3P_o}{(1-D)^2V_o}+\frac{V_{\mathrm{dr}3}DP_o}{V_o}+\frac{V_{\mathrm{dr}4}DP_o}{V_o}$$
$$+\frac{V_{\mathrm{dr}5}(1-D)P_o}{V_o}+\frac{V_{\mathrm{drS}}(D^3-D^2+D)P_o}{(1-D)^2V_o}. \quad (23)$$

The switching loss of the switch, namely, P_{S_S}, can be calculated as

$$P_{S\_S}\approx\frac{1}{2}\frac{D^3-D^2+D}{D^2(1-D)^2}P_o t_{\mathrm{off}}f_s \quad (24)$$

where t_{off} is the turning-off time of the switch.

Thus, the relatively accurate estimation of the efficiency η for the proposed converter can be obtained by using

$$\eta=\frac{P_o}{P_o+P_L+P_{\mathrm{DS}\_C}+P_{\mathrm{DS}\_dr}+P_{S\_S}}. \quad (25)$$

For quick estimation and roughly investigating the varying characteristics of the efficiency, it is assumed that the load R is large enough comparing to the parasitic resistors of the components and the turning-off time of the switch is short enough comparing to the switching period of the converter, then the expression of the efficiency can be simplified as shown in (26) by ignoring the joule effects losses of the inductors, the conduction losses of the diodes and the switch, and the switching loss of the switch and assuming the voltage drops of the diodes and the switch are equal to V_{drop}

$$\eta=\frac{V_gD^2-V_{\mathrm{drop}}(1+2D^3-D^2)}{V_gD^2}. \quad (26)$$

The relationship of the efficiency in regard to the input voltage and the duty cycle can be further illustrated in Fig. 8. It can be seen from (26) and Fig. 8 that the operating efficiency of the proposed converter is generally acceptable. Also, the higher operating efficiency can be obtained in the applications with higher input voltage. Additionally, the converter can operate more efficiently in step-up mode than in step-down mode as the efficiency of the converter will be increasing with the increase of the duty cycle.

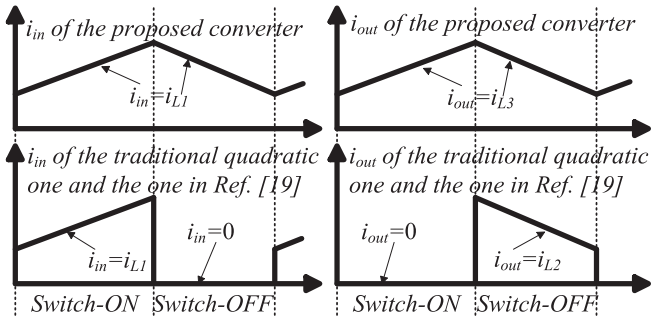

Fig. 9. i_{in} and i_{out} of the proposed converter and the traditional quadratic buck–boost converter.

IV. Performance Comparison

A. Comparison of Input and Output Currents Performance

Comparing the proposed converter with the traditional quadratic buck–boost converter and the converter proposed in [19], the voltage transformation ratios of these three converters are exactly the same. However, the input port current and output port current of them, namely, i_{in} and i_{out} as shown in Figs. 1 and 2, are different.

During the switch turned-ON mode, the input port current and output port current of both the traditional quadratic buck–boost converter and the converter proposed in [19] can be expressed as

$$i_{\mathrm{in}}=i_{L1},i_{\mathrm{out}}=0. \quad (27)$$

While those of the proposed converter can be expressed as

$$i_{\mathrm{in}}=i_{L1},i_{\mathrm{out}}=i_{L3}. \quad (28)$$

During the switch turned-OFF mode, the input port current and output port current of both the traditional quadratic buck-boost converter and the converter proposed in [19] can be expressed as

$$i_{\mathrm{in}}=0,i_{\mathrm{out}}=i_{L2} \quad (29)$$

while those of the proposed converter can be expressed as

$$i_{\mathrm{in}}=i_{L1},i_{\mathrm{out}}=i_{L3}. \quad (30)$$

Equations (27)–(30) can be clearly illustrated in Fig. 9, which shows that both the input port current and output port current of the traditional quadratic buck–boost converter and the converter proposed in [19] have a step change during the mode transition, which means that the current is discontinuous. The input port and output port currents of the proposed converter are always equal to the current of inductor L_1 and L_3, respectively, which indicates that the current is continuous.

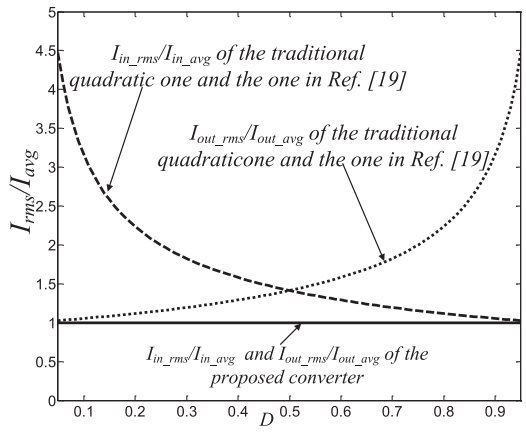

Fig. 10. $I_{\text{in\_avg}}/I_{\text{in\_rms}}$ and $I_{\text{out\_avg}}/I_{\text{out\_rms}}$ versus the duty cycle of the proposed converter and the traditional quadratic buck–boost converter.

Assuming the three converters operate under the same condition with the same average input port current $(I_{\text{in\_avg}})$ and output port current $(I_{\text{out\_avg}})$, the root-mean-square values of the input port current $(I_{\text{in\_rms}})$ and the output port current $(I_{\text{out\_rms}})$ of the traditional quadratic buck–boost converter and the converter proposed in [19] can be derived as

$$I_{\text{in\_rms}} = I_{\text{in\_avg}} \Big/ \sqrt{D}, I_{\text{out\_rms}} = I_{\text{out\_avg}} \Big/ \sqrt{(1-D)} \quad (31)$$

while those of the proposed converter are

$$I_{\text{in\_rms}} = I_{i\text{n\_avg}}, I_{\text{out\_rms}} = I_{\text{out\_avg}}. \quad (32)$$

Equations (31) and (32) show that the RMS values of both input port current and output port current of the proposed buck–boost converter are much smaller than those of the traditional quadratic buck–boost converter and the converter proposed in [19]. The difference can be clearly illustrated in Fig. 10, which shows $I_{\text{in\_avg}}/I_{\text{in\_rms}}$ and $I_{\text{out\_avg}}/I_{\text{out\_rms}}$ versus the duty cycle of these two converters.

B. Comparison of Other Features

The comparison of several other key features including the number of components, voltage stresses of the switch and diodes, the type of input port current and output port current of the proposed converter versus other converters including the traditional quadratic buck–boost converter and the converter proposed in [19] are summarized in Table I, in which all the expressions are derived by assuming that the components are ideal and the converters operate in continuous inductor current mode. From Table I, it can be found that the converter has two more diodes than the traditional quadratic buck–boost converter, which may slightly increase the cost of the converter. However, the proposed converter has much wider operating range than the traditional one. This is because that when the duty cycle is larger than 0.5, the voltage stress of the diode D_1 in the traditional quadratic buck–boost converter will become negative, which will result in malfunction of the converter. This fact will limit the traditional quadratic buck–boost converter only working in buck mode. Compared to the converter in [19], the proposed converter requires three more diodes. However, the proposed converter only applies one switch, while the converter in [19] requires two switches. Considering the related cost of the extra switch and its control and driving circuits, the increased cost by the three more diodes of the proposed converter compared to the converter proposed in [19] might be balanced. Although the proposed converter requires one more inductor and one more capacitor than the traditional quadratic buck–boost converter and the converter proposed in [19], the proposed converter has continuous input port current and continuous output port current while those of the other two counterparts are discontinuous, which may result in the demand for extra inductors and capacitors as input and output filters to satisfy the electromagnetic interference/electromagnetic compatibility issues in practical applications. Therefore, the cost of the proposed converter is generally acceptable comparing to the traditional one and the one proposed in [19].

V. Key Parameters Design

A. Parameters Design of Inductors

In practical applications, the current ripple is always preassigned. Therefore, the inductance of the inductors L_1, L_2, and L_3 can be obtained as

$$\begin{cases} L_1 = \dfrac{(1-D)^2 V_o}{D\Delta i_{L1} f_s} \\ L_2 = \dfrac{(1-D)V_o}{D\Delta i_{L2} f_s} \\ L_3 = \dfrac{(1-D)V_o}{\Delta i_{L3} f_s} \end{cases}. \quad (33)$$

At the same time, the inductances should satisfy the equations in (8) if the converter is designed to operate in the continuous inductor current mode.

B. Parameters Design of Capacitors

The capacitors are designed to control the voltage ripples of the capacitors, which can affect the stability of the converter, to an acceptable extent. The voltage ripples of the capacitors of the proposed converter, namely, Δv_{C1}, Δv_{C2}, and Δv_{C3} can be deduced as

$$\begin{cases} \Delta v_{C1} = \dfrac{D^2 I_o}{(1-D)C_1 f_s} \\ \Delta v_{C2} = \dfrac{DI_o}{C_2 f_s} \\ \Delta v_{C3} = \dfrac{V_o(1-D)}{8L_3 C_3 {f_s}^2} \end{cases}. \quad (34)$$

Similar to the parameter design of inductors, the voltage ripple is usually preassigned in practical applications. Therefore, the

TABLE I
COMPARISON BETWEEN THE PROPOSED CONVERTER AND THE EXISTING CONVERTERS

Topology		Traditional quadratic buck–boost converter		Converter proposed in [19]		Proposed converter	
Number of components	Inductors	2		2		3	
	Capacitors	2		2		3	
	Diodes	3		2		5	
	Switches	1		2		1	
Voltage conversion ratio		$\left(\frac{D}{1-D}\right)^2$		$\left(\frac{D}{1-D}\right)^2$		$\left(\frac{D}{1-D}\right)^2$	
Voltage stress of the switch		$\frac{1-D}{D^2}V_o$		S_1	$\frac{1-D}{D^2}V_o$	$\frac{1}{D^2}V_o$	
				S_2	$\frac{1}{D}V_o$		
Voltage stresses of the diodes	D_1	$\frac{1-2D}{D^2}V_o$		D_1	$\frac{1-D}{D^2}V_o$	D_1	$\frac{1-D}{D^2}V_o$
						D_2	$\frac{1}{D}V_o$
	D_2	$\frac{1-D}{D^2}V_o$		D_2	$\frac{1}{D}V_o$	D_3	$\frac{1}{D^2}V_o$
						D_4	$\frac{1-D}{D^2}V_o$
	D_3	$\frac{1}{D}V_o$				D_5	$\frac{1}{D}V_o$
Input port current type		Discontinuous		Discontinuous		Continuous	
Output port current type		Discontinuous		Discontinuous		Continuous	

capacitance of the capacitors can be designed as

$$\begin{cases} C_1 = \dfrac{D^2 I_o}{(1-D)\Delta v_{C1} f_s} \\ C_2 = \dfrac{D I_o}{\Delta v_{C2} f_s} \\ C_3 = \dfrac{V_o(1-D)}{8 L_3 \Delta v_{C3} {f_s}^2} \end{cases}. \tag{35}$$

C. Selection of the Diodes and the Switch

The selection of the switch and diodes is to determine the rated voltage and current stresses of them. According to the aforementioned analysis in Section III-C, the corresponding parameters of the power devices can be easily determined and appropriate devices can be chosen.

VI. EXPERIMENTAL RESULTS

For the sake of safety and equipment availability in the lab, a prototype supplied by a low input voltage has been implemented and tested to confirm the effectiveness and validity of the proposed converter. Some main specifications of the built prototype are listed as follows:

$C_1 = 47\mu$F, $C_2 = 47\,\mu$F, $C_3 = 220\,\mu$F,
$L_1 = 100\,\mu$H, $L_2 = 400\,\mu$H, $L_3 = 3$ mH,
$f_s = 40$ kHz, $V_{in} = 20$ V, R = 3– 70 Ω.

Additionally, the lab available MOSFET IRFP260N is used for the switch S and DSEP8-06As are used for the diodes $D_1 - D_5$. The switch S is driven by the IC of type TLP350. The detailed driving circuit can be referred to [19] as the function of the ICs TLP350 and TLP250 are similar to each other. A KEITHLEY power supply of type 2231-30-3 is used as the input source in the experimental work. The differential probes of type THDP0200 and the probes of type TPP0250 are used for measuring the voltage information while the current probes of type TCP0030A are used for measuring the current. All the experimental waveforms are recorded by the oscilloscope of type Tektronix MDO3024.

The experimental results of the converter operating in step-up mode with the duty cycle of 0.6 and a pure resistive load of 60 Ω are shown in Fig. 11. Fig. 11(a) shows that the output voltage is about 38.77 V, which is close to the calculated results. Fig. 11(b) shows that the voltages of the capacitors C_1 and C_2 are generally constant, about 45.87 and 68.55 V, respectively. The drain-source voltage of the switch is about 112 V, which is approximately equal to the sum of the voltages of the capacitors C_1 and C_2. The current waveform of the inductor L_1 presented in Fig. 11(a) and the current waveform of the inductor L_3 presented in Fig. 11(b) are noted to be continuous, which indicates the earlier analysis that the proposed converter has continuous input port current and output port current. The current waveforms presented in Fig. 11(a) and (b) show that the current flow through the switch is approximately equal to the sum of the three inductors' current when the switch is turned ON. Hence, the experimental results correspond well with the theoretical analysis. Similarly, Fig. 12 shows the experimental results obtained in step-down mode of the converter with a duty cycle of 0.4 and a pure resistive load of 6 Ω. The experimental waveforms are also corresponding well with the theoretical analysis. The features

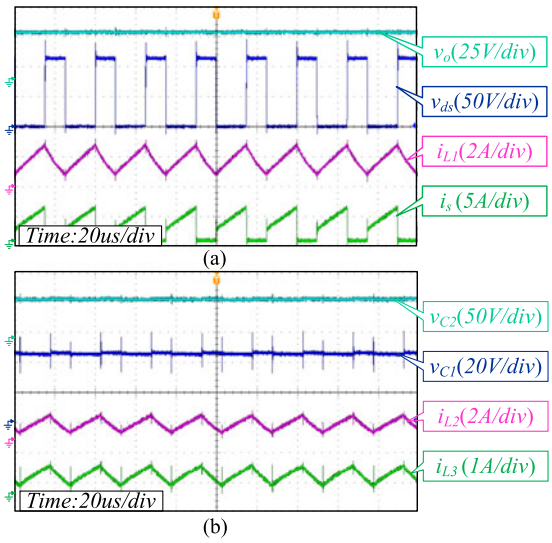

Fig. 11. Experimental results in step-up mode with D = 0.6 and R = 60 Ω: (a) voltage waveforms of output voltage and drain-source voltage of the switch S, current waveforms of the inductor L_1 and the switch S, (b) voltage waveforms of the capacitors C_1 and C_2, current waveforms of the inductors L_2 and L_3.

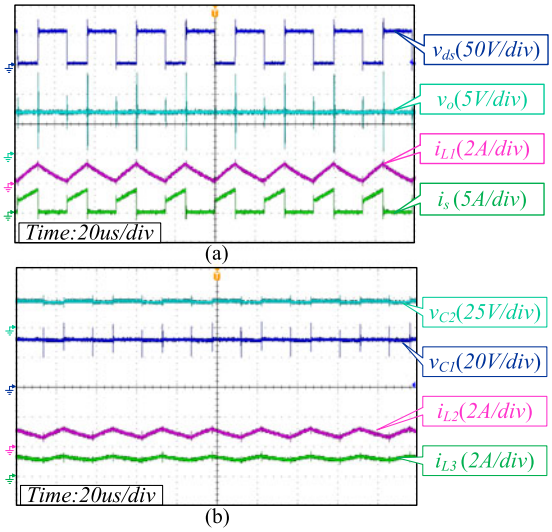

Fig. 12. Experimental results with D = 0.4 and R = 6 Ω: (a) voltage waveforms of output voltage and drain-source voltage of switch S, current waveforms of the inductor L_1 and the switch S, (b) voltage waveforms of the capacitors C_1 and C_2, current waveforms of the inductors L_2 and L_3.

of the proposed quadratic buck–boost converter are therefore verified.

In order to study the dynamic performance of the proposed converter, the built prototype was tested with step changes in the load and the results are shown in Fig. 13. Fig. 13(a) shows the converter response in step-up mode with the load changing from 60 to 45 Ω at point A. The output voltage is almost stable under this load variation, and the slight change is caused by the parasitic parameters of the components. Fig. 13(b) is the waveforms in step-down mode with load changing from 6 Ω to 4 Ω at point B. The results indicate that the dynamic characteristic of the converter is satisfied even in open-loop condition.

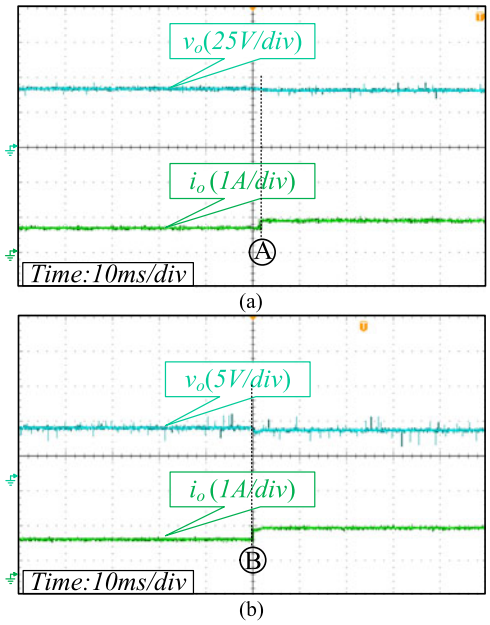

Fig. 13. Dynamic performance of the proposed converter in (a) step-up mode with the load changing from 60 to 45 Ω, (b) step down mode with the load changing from 6 to 4 Ω.

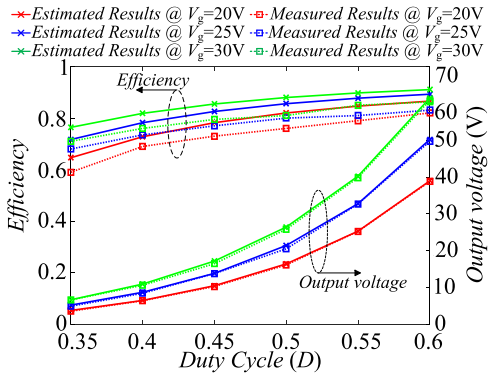

Fig. 14. Comparisons of the efficiency and output voltage of the converter between the experimental results and the theoretically estimated values.

The close-loop controller can be designed based on the transfer function of the converter, which can be easily derived by using the small-signal modeling method. The designing method of the controller proposed for other quadratic converters [4]–[8] can also be referred for designing the controller for the proposed converter.

The measured results of efficiency and output voltage from the built prototype under different operating conditions as well as the theoretically estimated values are shown in Fig. 14. Comparing to the theoretically estimated values, the measured results are generally acceptable. The efficiency increases with the increase of the duty cycle and the increase of the input voltage, which demonstrates the analysis in Section III-D. Since the maximum input voltage applied in the test is only 30 V, which is relatively low, and the parasitic parameters of the diodes and MOSFET used in the prototype are comparatively large, which

contribute to lots of power losses compared to the output power, the efficiency of the built prototype is not high enough. However, it is expectable that the efficiency of the converter can be effectively improved if the converter is applied in high-input voltage applications and built with better graded devices as analyzed in Section III-D.

VII. Conclusion

A novel single-switch quadratic buck–boost converter with continuous input port current and continuous output port current is proposed in this paper. The proposed converter is constructed by combining one traditional boost converter, one traditional buck–boost converter, and one traditional buck converter using only one switch. The proposed converter has an inductor in the input port as well as an inductor in the output port, which is capable of making the input port current and output port current to be continuous and contributes to the simplification of the design of input and output filters. The operating principle of the proposed converter operating in continuous inductor current mode is analyzed. This paper also analyzes the steady-state performance of the circuit and the design of the key parameters of the components. Experimental results from a prototype built in the lab are obtained to verify the effectiveness and the validity of the converter. This converter can be a good complement for the existing quadratic buck–boost converters and an appropriate candidate for industrial applications such as PV system and multifunction power supply.

References

[1] D. Maksimovic and S. Cuk, "General properties and synthesis of PWM DC-to-DC converters," in *Proc. IEEE Power Electron. Spec. Conf.*, 1989, pp. 515–525.

[2] D. Maksimovic and S. Cuk, "Switching converters with wide DC conversion range," *IEEE Trans. Power Electron.*, vol. 6, no. 1, pp. 151–157, Jan. 1991.

[3] G. Moschopoulos, "Quadratic power conversion for industrial applications," in *Proc. 25th Annu. IEEE Appl. Power Electron. Conf. Expo.*, 2010, pp. 1320–1327.

[4] X. L. Wei, K. M. Tsang, and W. L. Chan, "Non-linear PWM control of single-switch quadratic buck converters using internal model," *IET Power Electron.*, vol. 2, no. 5, pp. 475–483, Sep. 2009.

[5] J. A. M. Saldana, J. L. Ramos, E. E. C. Gutierrez, and M. G. O. Lopez, "Average current-mode control scheme for a quadratic buck converter with a single switch," *IEEE Trans. Power Electron.*, vol. 23, no. 1, pp. 485–490, Jan. 2008.

[6] J. J. Chen, B. H. Huang, C. M. Kung, W. Y. Tai, and Y. S. Hwang, "A new single-inductor quadratic buck converter using average-current-mode control without slope-compensation," in *Proc. 5th IEEE Conf. Ind. Electron. Appl.*, Jun. 2010, pp. 1082–1087.

[7] J. A. M. Saldana, R. L. Palomo, and E. P. Hernandez, "Parameters selection criteria of proportional–integral controller for a quadratic buck converter," *IET Power Electron.*, vol. 7, no. 6, pp. 1527–1535, Jun. 2014.

[8] A. Ayachit and M. K. Kazimierczuk, "Open-loop small signal transfer functions of the quadratic buck PWM DC-DC converter in CCM," in *Proc. 40th Annu. Conf. IEEE Ind. Electron. Soc.*, Nov. 2014, pp. 1643–1649.

[9] L. D. R. Barbosa, J. B. Vieira, L. C. D. Freitas, M. D. S. Vilela, and V. J. Farias, "A buck quadratic PWM soft-switching converter using a single active switch," *IEEE Trans. Power Electron.*, vol. 14, no. 3, pp. 445–453, May 1999.

[10] V. M. Pacheco, A. J. D. Nascimento, V. J. Farias, J. B. Vieira, and L. C. de Freitas, "A quadratic buck converter with lossless commutation," *IEEE Trans. Ind. Electron.*, vol. 47, no. 2, pp. 264–272, Apr. 2000.

[11] R. L. Palomo, J. A. M. Saldana, and E. P. Hernandez, "Quadratic step-down dc–dc converters based on reduced redundant power processing approach," *IET Power Electron.*, vol. 6, no. 1, pp. 136–145, Jan. 2013.

[12] J. L. Ramos, M. G. O. Lopez, L. H. D. Saldierna, and J. A. M. Saldana, "Switching regulator using a quadratic boost converter for wide DC conversion ratios," *IET Power Electron.*, vol. 2, no. 5, pp. 605–613, Sep. 2009.

[13] J. A. M. Saldana, R. L. Palomo, E. P. Hernandez, and J. L. G. Martinez, "Modelling and control of a DC–DC quadratic boost converter with R^2P_2," *IET Power Electron.*, vol. 7, no. 1, pp. 11–22, Jan. 2014.

[14] O. L. Santos, L. M. Salamero, G. Garcia, H. V. Blavi, and T. S. Polanco, "Robust sliding-mode control design for a voltage regulated quadratic boost converter," *IEEE Trans. Power Electron.*, vol. 30, no. 4, pp. 2313–2327, Apr. 2015.

[15] M. A. A. Saffar, E. H. Ismail, and A. J. Sabzali, "High efficiency quadratic boost converter," in *Proc. 27th Annu. IEEE Appl. Power Electron. Conf. Expo.*, 2012, pp. 1245–1252.

[16] Y. M. Ye and K. W. E. Cheng, "Quadratic boost converter with low buffer capacitor stress," *IET Power Electron.*, vol. 7, no. 5, pp. 1162–1170, May 2014.

[17] O. A. Rahim and H. Funato, "Switched inductor quadratic boosting ratio inverter with proportional resonant controller for grid-Tie PV applications," in *Proc. 40th Annu. Conf. IEEE Ind. Electron. Soc.*, 2014, pp. 5606–5611.

[18] G. Zhang *et al.*, "A 3-Z-network boost converter," *IEEE Trans. Ind. Electron.*, vol. 62, no. 1, pp. 278–288, Jan. 2015.

[19] S. Miao, F. Wang, and X. Ma, "A new transformerless buck-boost converter with positive output voltage," *IEEE Trans. Ind. Electron.*, vol. 63, no. 5, pp. 2965–2975, May 2016.

Neng Zhang photograph and biography not available at the time of publication.

Guidong Zhang (S'13–M'15) photograph and biography not available at the time of publication.

Khay Wai See photograph and biography not available at the time of publication.

Bo Zhang (M'05–SM'15) photograph and biography not available at the time of publication.